Molecular Crystals and Liquid Crystals

ISSN: 1542-1406 (Print) 1563-5287 (Online) Journal homepage: http://www.tandfonline.com/loi/gmcl20

Synthesis, X-Ray Structural, Characterization, NLO, MEP, NBO, and HOMO–LUMO Analysis Using DFT Study of Co(II)bis(3,4 dimethoxybenzoate)bis(nicotinamide) Dihydrate

Elif Çelenk Kaya, Zeynep Demircioğlu, Afşin Ahmet Kaya & Orhan Büyükgüngör

To cite this article: Elif Çelenk Kaya, Zeynep Demircioğlu, Afşin Ahmet Kaya & Orhan Büyükgüngör (2015) Synthesis, X-Ray Structural, Characterization, NLO, MEP, NBO, and HOMO–LUMO Analysis Using DFT Study of Co(II)bis(3,4 dimethoxybenzoate)bis(nicotinamide) Dihydrate, Molecular Crystals and Liquid Crystals, 609:1, 103-117, DOI: 10.1080/15421406.2014.927964

To link to this article: http://dx.doi.org/10.1080/15421406.2014.927964

Published online: 11 Apr 2015.

Mol. Cryst. Liq. Cryst., Vol. 609: pp. 103–117, 2015

ISSN: 1542-1406 print/1563-5287 online
DOI: 10.1080/15421406.2014.927964

Synthesis, X-Ray Structural, Characterization, NLO, MEP, NBO, and HOMO–LUMO Analysis Using DFT Study of Co(II)bis(3,4 dimethoxybenzoate)bis(nicotinamide) Dihydrate

ELIF ÇELENK KAYA,[1,*] ZEYNEP DEMİRCİOĞLU,[2] AFŞIN AHMET KAYA,[1] AND ORHAN BÜYÜKGÜNGÖR[2]

[1]School of Health, Gümüşhane University, Gümüşhane, Turkey
[2]Department of Physics, Faculty of Arts and Sciences, Ondokuz Mayıs University, Kurupelit-Samsun, Turkey

A suitable single crystal of Co(II)bis(3,4 dimethoxybenzoate)bis(nicotinamide) dihydrate, formulated as $C_{30}H_{38}N_4O_{14}Co$,(I). According to experimental data, the complex can be characterized in the solid state as mononuclear, with a distorted octahedral stereochemistry. The distorted octahedral stereochemistry adopted by the complex was further confirmed by the x-ray structure analysis of current study, which consists of a six-coordinate Co atom in a distorted octahedral environment constructed from two N atoms and four O atoms. The title compound which has been characterized by IR, UV, and single crystal X-ray diffraction analysis at 296 K crystallizes in the monoclinic space group C 2/c *with* a = *27.9402(15) Å,* b = *8.6005(3)Å,* c = *14.7921(9)Å,* $\alpha = 90^\circ$, $\beta = 108.849(4)^\circ$, *and* $\gamma = 90^\circ$, Z = *4. The molecular structure and geometry have also been optimized using B3LYP density functional theory method employing the 6-31G (d) basis set. The molecular electrostatic potential (MEP), frontier molecular orbitals (FMO) analysis, nonlinear optical properties (NLO), and natural bond analysis (NBO) for the title molecule are also described from the computational process.*

Keywords Density functional theory (DFT); frontier molecular orbitals; molecular electrostatic potential (MEP); nicotinamide; nonlinear optical properties (NLO); X-ray analysis

1. Introduction

Nicotinamide (nia) and nicotinic acid (nic) are two of most extensively studied pyridine derivatives. The former is a component of the vitamin B complex and of the vital coenzyme NAD (nicotinamide adenine dinucleotide) [1]. Nicotinamide (nia) and nicotinic acid (nic) are two of the most extensively studied pyridine derivatives. The former is a component of the vitamin B complex and of the vitalcoenzyme NAD (nicotinamide adenine dinucleotide) [2]. Furthermore, early administration of nicotinamide has been reported to impair learning and memory in mice [3]. The medicinal chemistry of nicotinamide in the treatment of

*Address correspondence to Elif Çelenk Kaya, School of Health, Gümüşhane University, TR-29000 Gümüşhane, Turkey. Fax: 00 90 (0456)-233 73 22. E-mail: elifcelenk1629@hotmail.com

Color versions of one or more of the figures in the article can be found online at www.tandfonline.com/gmcl.

ischemia and reperfusion has also developed rapidly in the past few years. Nicotinic acid has a wide-ranging ability to reduce lipid levels, but its clinical uses are restricted due to its various side effects. Nicotinic acid and nicotinamide form niacin, a water-soluble vitamin that reduces VLDL cholesterol and increases HDL cholesterol (the so-called "good" cholesterol) [4]. Moreover, coordination compounds of nicotinic acid, nicotinamide, and their derivatives are known to have antiviral or antibacterial activity [5, 6], and they also selectively affect tumor tissues [7].

In recent decades, metallocomplexes have received much attention in chemistry, biochemistry, and pharmacyas promising compounds for the creation of novel drugs. On the one hand, using such complexes, it is possible to avoid some negative effects inherent in drug compositions containing inorganic salts, which can dissociate with the formation of metal ions. On the other hand, metal ions can modify both magnitude and direction of the pharmacological activity of the initial organic compounds (ligands) as a result of changes in their size, shape, charge density distribution, and redox potentials [8]. During recent years coordination compounds of biologically active ligands have received much attention and it has been reported that chelation causes drastic change in the biological properties of the ligands and also the metal moiety, moreover, many drugs possess modified pharmacological and toxicological properties when administered in the form of transition metal complexes [9–11].

In this paper, we report the molecular and crystal structure of Co(II)bis(3,4 dimethoxybenzoate)bis(nicotinamide) dihydrate (Fig. 1), together with the IR, and single crystal X-ray diffraction studies. Besides these, the molecular structure and geometry, FMOs, MEP, NBO, total molecular energies, and dipol moments have also been studied using the DFT/ B3LYP employing the 6-31G(d) basis set. The results obtained from theoretical calculations and experiments are compared in this study.

2. Experimental

2.1. Synthesis

The title compound was prepared by the reaction of $CoCl_2.6H_2O$ (0.67 g, 2.8 mmol) in H_2O (50 ml) and nicotinamide (0.68 g, 5.6 mmol) in H_2O (10 ml), with sodium 3,4 dimethoxybenzoate (1.02 g, 5.6 mmol) in H_2O (50 ml), at room temperature. The mixture was filtered and set aside to crystallize at ambient temperature for one week, giving orange single crystals. M.p.118–119°C. IR (ATR sampling accessory-ν max/cm^{-1}): 3232, 2163, 1677, 1624, 1515, 1412, 1373, 1259, 1271, 1113, 1023, 767, 684, and 633. Anal. Calcd for $C_{30}H_{34}CoN_4O_{12}$: C, 51.36; H, 4.88; N, 7.99; Found: C, 51.40; H, 4.82; N, 8.09%. MS: 702 [M^++1].

2.2. Instrumentation

The FT-IR spectrum of the title compound was recorded in the 4000–400 cm^{-1} region with a Bruker Vertex 80V FT-IR spectrometer using KBr pellets. Absorption spectra were determined on Unicam UV-Vis spectrometer.

2.3. X-Ray Crystallography

The single-crystal X-ray data were collected on a STOE IPDS II image plate diffractometer at 296 K. Graphite-monochromated Mo K_α radiation (λ = 0.71073 A) and the w-scan

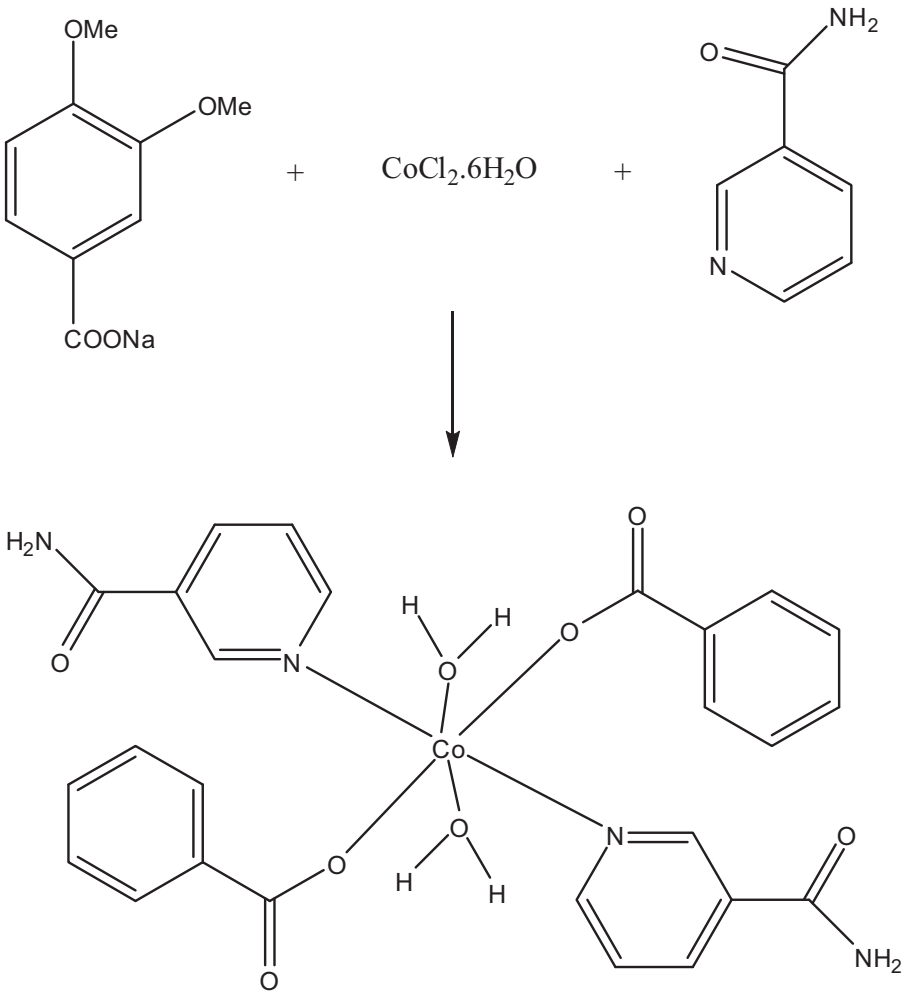

Figure 1. Chemical diagram of Co(II)bis(3,4 dimethoxybenzoate)bis(nicotinamide) dihydrate.

technique were used. The structure was solved by direct methods using SHELXS-97 [12] and refined through the full-matrix least-squares method using SHELXL-97 [13], implemented in the WinGX [14] program suite. Nonhydrogen atoms were refined with anisotropic displacement parameters. All H atoms were located in a difference Fourier map and were refined isotropically. Data collection: Stoe X-AREA [14], cell refinement: Stoe X-AREA [33], data reduction: Stoe XRED [15]. The general-purpose crystallographic tool PLATON [16] was used for the structure analysis and presentation of the results. The structure was refined to $R_{\text{int}} = 0.028$ with 3075 observed reflections using $I > 2\sigma(I)$ threshold. The program ORTEP-3 [14] for Windows was used preparation of the figures. Details of the data collection conditions and the parameters of the refinement process are given in Table 1.

Table 1. Crystal data and structure refinement parameters for the title compound

Chemical formula	$C_{30}H_{38}N_4O_{14}Co$
Color/shape	Brown/Plate
Formula weight	737.57
Temperature	296 K
Crystal system	Monoclinic
Space group	*C 2/c*
Unit cell parameters	$a = 27.9402(15)$Å
	$b = 8.6005(3)$Å
	$c = 14.7921(9)$Å
	$\alpha = 90$å
	$\beta = 108.849(4)$å
	$\gamma = 90$å
Volume	3363.9(3)Å^3
Z	4
Density	1.456 g/cm^3
Absorption coefficient	0.584 mm^{-1}
Diffractometer/meas. meth.	STOE IPDS 2/ϖ-scan
θ range for data collection	2.5å to 26.5å
Unique reflections measured	24588
Total reflection/observed reflections	3489/ 3075
Goodness of fit on F^2	1.053
Final R indices [$I > 2\sigma(I)$]	$R_1 = 0.029$, $wR_1 = 0.073$
R indices (all data)	$R_2 = 0.036$, $wR_2 = 0.076$

2.4. Computational Details

The entire calculations conducted in the present work were performed at B3LYP levels included in the Gaussian 03Wpackage [17] program together with 6–31G(d) basis set function of the density functional theory (DFT) utilizing gradient geometry optimization [18]. Initial geometry generated from standard geometrical parameters was minimized without any constraint in the potential energy surface at Hartree–Focklevel, adopting the standard 6–31G(d) basis set. This geometry was reoptimized again at B3LYP level, using basis set 6–31G(d) for better description. The optimized structural parameters were used in the vibrational frequency calculations at the DFT levels to characterize all stationary points as minima. At the optimized structure of the examined species, no imaginary frequency modes were obtained proving that a true minimum on the potential energy surface was found. We have utilized the gradient corrected DFT [19] with the three parameter hybrid functional (B3) [20] for the Exchange part and the Lee-Yang-Parr (LYP) correlation function [21], accepted as a cost effective approach for the computation of molecular structure, energies of optimized structures. By combining the results of the Gauss view program [22] with symmetry considerations were made with a high degree of accuracy. The natural bonding orbitals (NBO) calculations [23] were performed using NBO 3.1 program as implemented in the Gaussian 03W [17] package at the DFT/B3LYP/6–1G(d) level in order to understand various second-order interactions between the filled orbitals of one subsystem and vacant orbitals of another subsystem, which is a measure of the intramolecular delocalization or hyper conjugation. Highest occupied molecular orbital (HOMO) and lowest-lying unoccupied

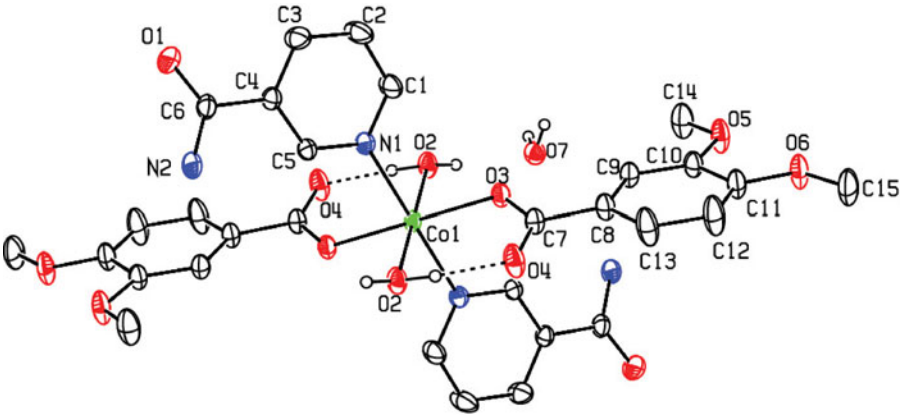

Figure 2. Ortep 3 diagram for Co(II)bis(3,4 dimethoxybenzoate)bis(nicotinamide) dihydrate, with the atom numbering scheme. Dashed lines show the O—H . . . O intra molecular hydrogen bonds.

molecular orbital (LUMO) analysis have been used to elucidate the information regarding charge transfer within the molecule. Molecular electrostatic potential (MEP) analysis has been used to find the reactive sites of the compound. In addition, the nonlinear optical (NLO) properties were computed at the theory level and the title compound showed a good second order nonlinear optical property. The energy gap between HOMO and LUMO has an important role in getting polarizability of a molecule. The increment of the strength of the donor and acceptor groups increases the NLO properties of organic molecules due to the decrease the energy gap between HOMO and LUMO. Because of this result, NLO analyses are vital importance for the metal organic molecules.

3. Results and Discussion

3.1. Description of the Crystal Structure

In the title compound, $C_{30}H_{38}N_4O_{14}Co$, the Co ion is located on a crystallographic inversion center. The Co center locates on the inversion center and coordinates the two oxygen atoms from two 3,4 dimethoxybenzoate, two nitrogen atoms from two nicotinamide, and two oxygen atoms from a pair of water molecules to form an octahedral geometry. The equality of the bonds which are positioning at the symmetric location Co-N1 [2.1332(13) Å; 2.1332(13) Å]; Co-O3 [2.0960(13) Å; 2.0960(11) Å]; Co-O2 [2.0823(12) Å; 2.0823(12) Å] bonds in the carboxylate group indicates a delocalized bonding arrangement, rather than localized single and double bonds. These values are satisfactory agreement with found of those in the literature [24, 25]. As a result of the delocalization of the electron density Co ion surrounding, O3-Co1-N1, N1-Co1-O2, C1-N1-Co1, and C7-O3-Co1 angles are 93.65(5), 87.24(5), 120.7(10), and 129.19(10)°, respectively.

The Co centre in complex (I) displays a slightly distorted octahedral coordination and lies on an inversion centre. The Co centre is coordinated by two O atoms [O2 and O2i;symmetry code: (i) (1/2-x,3/2-y,1-z) and two O3 atoms (O3and O3i) of two water, and by two N atoms (N1 and N1i) of two coordinated nicotinamide molecules (Fig. 2).

Table 2. Hydrogen bonding geometry for the title compound

D-H···A	D-H	H···A	D···A	D-H···A
O2-H5b···O4	0,94(3)	1.70(3)	2.6085(19)	162(3)
O7-H7a . . . O1^{i}	0.81(3)	2.06(3)	2.853(2)	167(3)
N2 -H2c . . . O5^{ii}	0.86	2.11	2.906(2)	153

Symmetry codes: (i) 1/2−*x*,-1/2+*y*,1/2−*z*; (ii) 1/2+*x*,−1/2+*y*,*z*.

The dihedral angle between 3,4 dimethoxybenzoate groups ring A (C1-C5, N1) and nicotinamide groups ring B (C8-C13) is 77.03(7)° [both nearly planar with r.m.s deviations of 0.0236(12) Å for C4 and 0.0091(13) Å for C9 from the mean planes]. The two C−O−CH_3 groups are antisymmetric with respect to centroid of benzene ring B(C8-C13). This groups dihedral angles are 118.02(15)° and 118.30(13)° for C11-O6-C15 and C10-O5-C14, respectively.

An intramolecular O2-H2b . . . O4 contact leads to the formation of a six-membered ring with graph-set descriptor S(6) [26]. This bonding atoms of O2' s position is (*x*, *y*, *z*) but the others of O4 and H4B atoms are located at (1/2-*x*, 3/2-*y*,1-*z*).In the crystal, molecules are linked into dimers via O−H . . . O hydrogen bonds (Table 2). The crystal packing is also stabilized by N−H . . . O hydrogen bonds (Fig. 3).

3.2. Theoretical Structure

Some structural parameters obtained experimentally and calculated theoretically by B3LYP/631G (d) are given in Table 3 for comparison. The differences observed between the

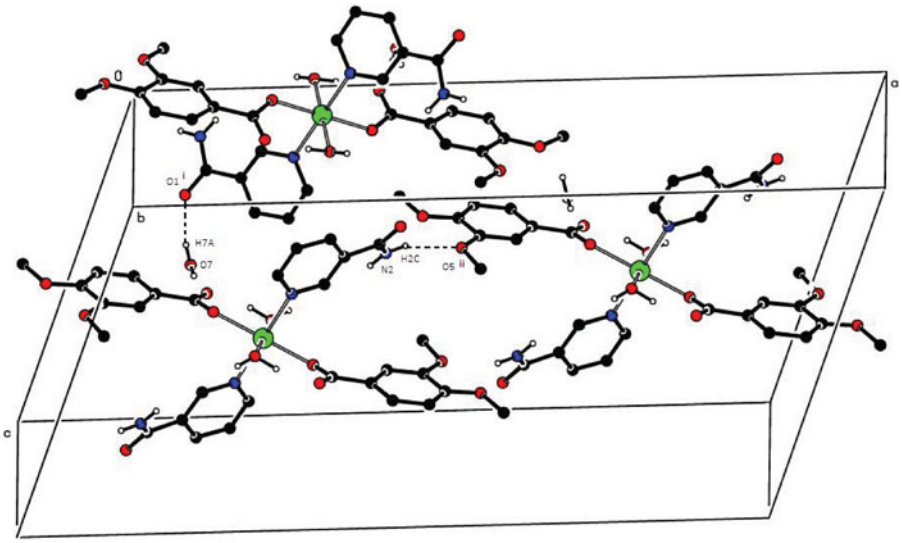

Figure 3. A packing diagram for (*I*), showing the O-H···O, N-H . . . O hydrogen bonds. H atoms not involved in hydrogen bonding (dashed lines) have been omitted for clarity. [Symmetry codes: (i) 1/2-*x*,−1/2+*y*,1/2−*z*;(ii) 1/2+*x*,−1/2+*y*,*z*.]

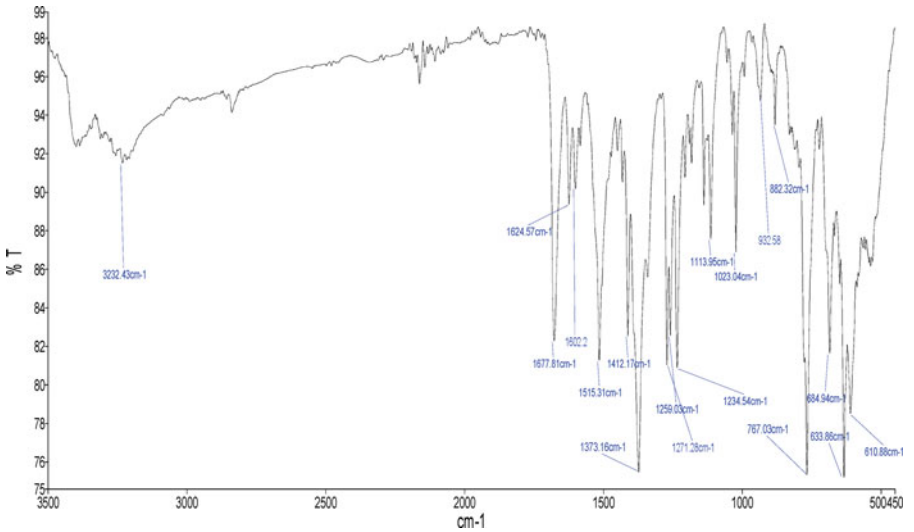

Figure 4. IR spectrum of the title compound.

Table 3. Selected molecular structure parameter for the title compound

	X-ray	DFT		X-ray	DFT
Bond lengths (Å)			Bond angles (°)		
Co1-N1	2.1332(13)	1.8189	C7-O3-Co1	129.2(10)	88.847
Co1-O3	2.0960(11)	1.9261	O3-Co1-N1	93.65(5)	100.5532
Co1-O2	2.0823(12)	1.9573	C8-C7-O3	117.5 (14)	122.4342
C7-O3	1.2574(19)	1.2748	C13-C8-C7	121.4(15)	120.9143
C7-C8	1.502(2)	1.4678	C15-O6-C11	118.2(15)	115.7386
C11-O6	1.3616(19)	1.3568	C14-O5-C10	118.3(15)	117.7115
C10-O5	1.3612(19)	1.3612	O6-C11-C12	125.5(12)	115.6397
C4-C6	1.501(2)	1.5027	O5-C10-C9	125.5(14)	125.2231
C6-N2	1.319(2)	1.3747	O1-C6-N2	122.8(15)	121.8036
C6-O1	1.228(2)	1.2244	C4-C6-N2	117.2(13)	116.5056
C7-O4	1.258(2)	1.293	C4-C6-O1	120.1(15)	121.674
C15-O6	1.427(2)	1.4194	C1-N1-Co1	120.7(10)	119.8536
C14-O5	1.416(2)	1.419	O2-Co1-O3	89.43(5)	163.432
C1-N1	1.329(2)	1.3665	O2-Co1-N1	87.24(5)	95.9808
Torsion angles (°)					
C7-O3-Co1-N1	−70.67(14)	−176.1626	C5-N1-Co1-O3	−140.1(12)	160.5375
O1-C6-N2-H2c	−0.86(2)	−9.1632	C14-O5-C10-C9	−6.0(3)	0.0537
O2- Co1-O3-C7	16.52(14)	2.5635	C15-O6-C11-C12	−5.0(3)	−0.0475
C13-C12-C11-O6	−178.8(2)	−179.9401	C13-C8-C7-O3	171.1(19)	176.617
O3-Co1-N1-C1	42.37(15)	−17.1927	Co1-O3-C7-C8	159.3(11)	158.5943

experimental and calculated parameters are due to the ignored effects. These effects are the intermolecular interactions which the theoretical methods can not take into account. While the experimental results belong to the solid state, the calculated results belong to the isolated gaseous phase. Namely, the optimized geometry with B3LYP is preferred more planar conformation than X-ray geometry.

For the experimental and theoretical results harmony, we used the geometry from the title molecule, while calculate other parameters such as UV, MEP, frontier molecular orbitals (FMOs), Natural Bond Orbital (NBO) analysis and NLO properties.

3.3. Vibrational Spectra

In FT-IR spectra of the Co(II) complex OH absorption bands of aqua ligand is present in a range of 3232 cm^{-1} corresponding to stretching vibrations of water molecule. The complex give rise to strong band responsible for the C=O stretching. Conjugation between the carbonyl group and amide nitrogen causes small frequency shifts. The strong band observed at 1677 cm^{-1} is assigned to this mode. Pyridine ring vibrations of free nicotinamide at 1515 cm^{-1} shifts to lower frequencies in the spectrum of the metal complex. The shift is shown in range of 1412 cm^{-1}, approximately this can indicate that the pyridine ring is coordinated. The main difference in the spectrum of 3,4-dimethoxybenzoic acid is that the C=O stretching vibration of the carboxyl group at 1725 cm^{-1} is shifted to lower frequency in the metal complex. The absorption bands of carboxylate in the metal complex are observed in a range of 1677 cm^{-1}. This can be a consequence of coordination that takes place through the carboxyl group by deprotonation of the 3,4-dimethoxybenzoic acid molecule during coordination. The $\nu_s(COO^-)$ band is located at 1515 cm^{-1} for the Co(II) complex. The $\nu_{as}(COO^-)$ peak is observed at 1373 cm^{-1} for Co(II) complex. The OH bending peak for the 3,4-dimethoxybenzoic acid remained almost in the same position at 1271 cm^{-1} in the metal complex. The low-intensity bands in a region of 600–400 cm^{-1} are attributed to the M−N and M−O vibrations (Figure 4).

3.4. Electronic Absorption Spectra

The electronic absorption bands which have azo groups obtained from UV-Vis spectroscopy. We have also calculated electronic absorption spectra of Co(II) complex in solvent (Chloroform, Benzene, Ethanol, and DMSO) and using TD-DFT at B3LYP/631G(d) level by adding the polarizable continuum model (PCM). In the evaluation of the results was based on the oscillator strengths (f-value) which greater than 0.1. It is well known that $\pi \rightarrow \pi^*$ transition is shifted to long wavelength with increasing the solvent polarity. The reason of this shifting, the dipole moment of solvent is produced dipole moment over the solute matter. Consequently, the energy of the π^* orbital is decreased. Using different polarity of the solvents in the itle molecule, excitation energies also decrease absorption wavelengths with increasing the polarity. As can be seen from Table 4, while excitation energies decrease absorption wavelengths increase with increasing polarity of the solvents in the title molecule too. According to Table 4, we can say that the total energy decreases with the increasing polarity of the solvent. The lessening in total energy of the title molecule increases the stability. On the other hand, the energy gap (ΔE) between the HOMO and the LUMO and dipole moment increase with the polarity of the solvent. Charge delocalization of the molecule increases with the increasing polarity of solvent, therefore causes the dipole moment to be raised.

Table 4. Calculated energies, dipole moments, and frontier orbital energies for the title compound

	Gas phase ($\varepsilon = 1$)	Benzene ($\varepsilon = 2.3$)	Chloroform ($\varepsilon = 4.9$)	Ethanol ($\varepsilon = 24.3$)	DMSO ($\varepsilon = 46.7$)
E_{TOTAL} (eV)	−2601.77813881	−2601.79695552	−2601.7588316	−2601.76635286	−2601.76671971
E_{HOMO} (eV)	−3.663602	−3.722326	−3.755566	−3.312703	−3.787144
E_{LUMO} (eV)	−1.145118	−1.228772	−1.27697	−1.312703	−1.319074
ΔE (eV)	2.51	2.493554	2.478596	2.464469	2.46807
μ (D)	4.3759	5.1272	4.3656	4.3891	4.3706

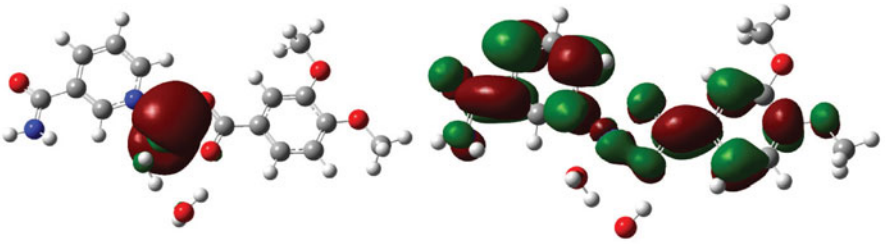

Figure 5. Molecular orbital surfaces and energies for the HOMO and LUMO of the title compound.

In the calculated UV-Vis spectrum of the title molecule absorption bands occur at 950.74, 959.72, 968.8, and 967.74 nm for benzene, chloroform, ethanol, and DMSO, respectively. These are arising from HOMO→ LUMO transition.

3.5. Frontier Molecular Orbitals

The HOMOs and the LUMOs are named as FMOs. The FMOs play an important role in the electric and optical properties, as well as in UV-Vis spectra and chemical reactions [27]. The distributions of the HOMO and LUMO orbitals computed at the B3LYP/6-31G (d) level for the title molecule are illustrated in Fig. 5. The calculations indicate that the title compound have 103 occupied MOs. While the LUMO is localized on almost the whole molecule, HOMO is localized on the Co ion and nicotinamide group, respectively. Both the HOMOs and the LUMOs are mostly π-antibonding type orbitals. Since the HOMO-LUMO energy separation has been used as a simple indicator of kinetic stability, it can be said that the title molecule which has a large HOMO-LUMO gap, 2.51 eV, implies low kinetic stability and high chemical reactivity [28, 29]. The HOMO–LUMO calculations show that the first hyperpolarizability of these derivatives is directly related to the HOMO–LUMO energy gap. Low value of the HOMO-LUMO energy gap is not surprising for the result of the high first hyperpolarizability. It is also associated with the too much positive partial charges on the whole of molecule.

3.6. Molecular Electrostatic Potential

MEP is related to the electronic density and is a very useful descriptor in understanding sites for electrophilic attack and nucleophilic reactions as well as hydrogen bonding interactions [30, 31]. The value of the MEP, $V(r)$, created by a molecular system at a point r gives the electrostatic energy on a unit positive charge located at r. The electrostatic potential $V(r)$ is also well suited for analyzing processes based on the "recognition" of one molecule by another, as in drug-receptor, and enzyme substrate interactions, because it is through their potentials that the two species first "see" each other [32, 33]. Experimental $V(r)$ computed with electron densities obtained from X-ray diffraction data has been used to explore the electrophilicity of hydrogen bonding functional groups [34]. Being a real physical property $V(r)$ can be determined experimentally by diffraction or by computational methods [35]. In the majority of the MEPs, while the maximum positive region which preferred site

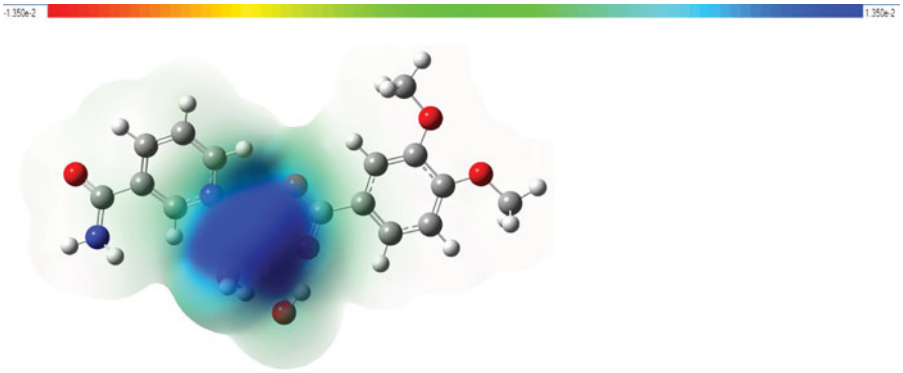

Figure 6. Molecular electrostatic potential map calculated at B3LYP/6-31G(d).

for nucleophilic attract indications as blue color, the maximum negative region which preferred site for electrophilic attract indications as red color. The study of experimental and theoretical $V(r)$ shows that H-donor and H-acceptor properties of molecules are revealed by positive and negative regions, respectively, so that the formation of a H-bond can be regarded as the consequence of a complementarity between the electrostatic potentials [36].

In the present study, the MEP of Co(II)bis(3,4 dimethoxybenzoate)bis(nicotinamide) dihydrate depicted in Fig. 6. Negative regions are associated with O7, O2, O3, O4, and N1 with values around −0.737567, −0.768142, −0.646154, −0.574169, and −0.573021 a.u., respectively. So, it is expected that the most preferred region for electrophilic attack is that around O6. However, the most maximum positive region is localized on atom C6, C7, C11, Co, and H2b with values are 0.486586, 0.564405, 0.332439, 0.453709, and 0.455239 a.u., respectively. Therefore, it would be predicted that the preferred site for nucleophilic attack will be C7. MEP figure shows no negative regions on the whole molecule (figure indicate no red locality), so there is no crystal structure, chemical activity. The Mulliken Population analysis support the partial positive regions become localized on the Co and N1 atoms and the figure shows them obviously. These atoms are the most positive regions for the molecule and these are preferred site for nucleophilic attract. The present study is vital importance because of the chemical and physical properties for researchers.

3.7. Natural Bond Orbital Analysis

NBO analysis provides an efficient method for studying intra- and intermolecular bonding and interaction among bonds, and also provides a convenient basis for investigation charge transfer or conjugative interactions in molecular system [37]. Another useful aspect of NBO method is that it gives information about interactions in both filled and virtual orbital spaces that could enhance the analysis of intra- and intermolecular interactions. The second-order Fock matrix was carried out to evaluate the donor–acceptor interactions in the NBO analysis [38]. For each donor NBO (i) and acceptor NBO(j), the stabilization energy associated with i

$\rightarrow j$ delocalization can be estimated as,

$$E(2) = \Delta E_{ij} = q_i \frac{F(i, j)^2}{\varepsilon_i \varepsilon_j}$$

Table 5. Significant donor–acceptor interactions of Co(II)bis(3,4 dimethoxybenzoate)bis (nicotinamide) dihydrate and their second-order perturbation energies calculated at B3LYP level using 6 -31G(d) basis set

Donor NBO(i)	Acceptor NBO(i)	$E(2)$[a] (kcal/mol)	$E_j - E_i$[b] (a.u.)	$F(ij)$[c] (a.u.)
C1-H1	C2	1.30	1.78	0.043
C1-C2	C3	1.91	1.48	0.048
C1-C2	N1	0.86	1.91	0.036
C1-N1	C1-C2	1.30	1.40	0.038
C1-H3	C1	0.82	1.56	0.032
C1-N1	C2	0.67	1.56	0.041
C3-H3	C1-N1	5.36	1.01	0.066
C2-C3	C4	2.29	1.95	0.06
C2-C3	C1-H1	2.28	1.19	0.046
C5-H5	C2	0.99	1.78	0.038
C5-H5	C1-C2	3.36	1.11	0.055
C3-C4	C5	0.68	1.53	0.029
C3-H3	C2-C3	0.42	1.10	0.027
C3-C4	C2-H2	1.22	1.17	0.048
C4-C6	C3	1.68	1.93	0.051
C4-C6	O1	1.13	1.89	0.042
C5-N1	C1-N1	1.52	1.3	0.04
O1	C6	15.59	1.48	0.136
C1-N1	C1	3.84	1.04	0.108
N2	C6-O1	0.52	14.79	0.078
N2	C6-O1	1.93	0.86	0.038
C6	N2-H2c	0.60	10.63	0.071
C1-N1	Co1	0.05	2.57	0.011
C5-N1	C7	0.07	2.97	0.013
C1-H1	C6-O1	4.05	0.54	0.108

[a]$E(2)$ means energy of hyperconjucative interactions.
[b]Energy difference between donor and acceptor i and j NBO orbitals.
[c]$F(i,j)$ is the Fock matrix element between i and j NBO orbitals.

where q_i is the donor orbital occupancy, ε_i, ε_j are diagonal elements(orbital energies) and F(i, j) is the off-diagonal NBO Fock matrix clement. In Table 5, the perturbation energies of significant donor–acceptor interactions are presented. The larger the E(2)value, the intensive is the interaction between electron donors and electron acceptors.

3.8. Nonlinear Optical Effects

Molecular materials with NLO properties are currently attracting considerable attention because of their potential applications in optoelectronic devices of telecommunications, information storage, optical switching, and signal processing. Comparing with organic molecules, metal complexes can offer great scope for the creation of multifunctional NLO materials. Recently, various multidimensional NLO metal complexes have emerged as

candidates for second-order NLO materials because of their potential advantages over one-dimensional chromophores, such as increasing β responses without undesirable losses of transparency in the visible region, possessed better phase-matching because of their larger off-diagonal components [39]. Metal complexes also display high environmental stability as well as considerable NLO responses [40], and thus become important choices for NLO materials [41–45].

Organometallic and coordination chemistry can offer a very large variety of molecular and bulk NLO structures in relation to the metal and configuration, oxidation state, spin state, etc. The central metal atom of an organometallic complex can readily coordinate to conjugated ligands and undergo p-orbital overlap facilitating effective electronic communication is leading to large dipole moment changes between the excited states.

The output from GAUSSIAN03W provides 10 components of the $3 \times 3 \times 3$ matrix as βxxx; βxxy; βxyy; βyyy; βxxz; βxyz; βyyz; βxzz; βyzz; βzzz; respectively, from which the x; y; and z components of β are calculated as described earlier [46]. When reporting a single value of β; one of the common formats is to simply treat the three independent values for β as a quasi Pythagorean problem and solve for the average β by the following equation.

$$\beta_{\text{top}} = \sqrt{\beta_x^2 + \beta_y^2 + \beta_z^2} \tag{1}$$

The total static dipole moment μ, the average linear polarizability α, and the first hyperpolarizability β can be calculated by using Eqs. (2)–(4), respectively,

$$\mu = \left(\mu_x^2 + \mu_y^2 + \mu_z^2\right)^2 \tag{2}$$

$$\alpha = \frac{1}{3}\left(\alpha_{xx} + \alpha_{yy} + \alpha_{zz}\right)^2 \tag{3}$$

$$\beta_{\text{tot}} = \left[\left(\beta_{xxx} + \beta_{xyy} + \beta_{xzz}\right)^2 + \left(\beta_{yyy} + \beta_{yzz} + \beta_{yxx}\right)^2 + \left(\beta_{zzz} + \beta_{zxx} + \beta_{zyy}\right)^2\right]^{1/2} \tag{4}$$

The dipole moment, polarizability and the first hyperpolarizability were calculated using polar = ENONLY at the level of B3LYP/6-31G(d) and the results obtained from calculation. The calculated polarizability αą and first hyperpolarizability β of I are 42.98 $A^{\circ 3}$ and 5.91×10^{-29} cm^5/esu that are greater than those of urea (α and β of urea of 3.8312 $A^{\circ 3}$ and 0.37289×10^{-30} cm^5/esu), respectively [47, 48].

The polar properties of the title molecule were calculated at the B3LYP/6-31G (d) level using the Gaussian 03W program package. The calculated values of electronic dipole moment, μ, polarizability, α, and the first hyperpolarizability, β for the title compound are, 1.7218 Debye, 42.98 $A^{\circ 3}$, 5.91×10^{-29} esu, respectively. It is well known that the substituents influence the polarity of the molecules. The high value of the first hyperpolarizability of the title compound can be seen a result of the metal complexes and surely become the optical material candidate.

4. Conclusion

In this study, we have performed the density functional calculations on Co(II)bis(3,4 dimethoxybenzoate)bis(nicotinamide) dihydrate starting from the X-ray geometry. Our objectives were to reproduce the molecular geometry, investigate the energetic behavior, reactive sites, delocalization of electron density, energy gap and NLO properties, and to comment the experimental IR and UV–vis data of the title molecule for the further studies.

According to this study, the calculated results for the molecular geometry show a good agreement with the results from X-ray diffraction. The total energy of the molecule decreases with the increasing polarity of the solvent and the stability of the molecule increases in going from the gas phase to the solution phase. The MEP map shows that the negative potential sites are on the electronegative atoms as well as the positive potential sites are around the Co, N1, and hydrogen atoms. But on the whole molecule shows no negative potential sites, so it is so amazing for the chemical activity. These sites give information about the possible areas for inter- and intramolecular hydrogen bonding. NBO analysis indicates the strong intramolecular interactions and in an agreement with the experimental intramolecular hydrogen bonding results. Natural bond orbital analysis of the molecule confirms that the intramolecular charge transfer caused by π-electron cloud movement from donor to acceptor must be responsible for the nonlinear optical properties of the title compound. Low HOMO-LUMO energy gap and high partial positive regions support the molecule for high first hyperpolarizability value, so its make the strong optical material applicant. We hope the results of this study will help researchers to design and synthesis new metal materials.

5. Supplementary Data

CCDC 948520 contains the supplementary crystallographic data for this paper. These data can be obtained free of charge via www.ccdc.cam.ac.uk/data_request/cif, by emailing data_request@ccdc.cam.ac.uk, or by contacting The Cambridge Crystallographic Data Centre, 12, Union Road, Cambridge CB2 1EZ, UK; fax: +44 1223 336033.

Acknowledgment

The authors wish to acknowledge the Faculty of Arts and Sciences, Ondokuz Mayis University, Turkey, for the use of the STOE IPDS 2 diffractometer (purchased under grant F.279 of the University Research Fund).

References

[1] Miwa, Y., Mizuno, T., Tsuchida, K., Taga, T., & Iwata, Y. (1999). *Acta Crystallogr., Sect. B.*, *55*, 78–84.
[2] Aakeröy, C. B., & Beatty, A. M. (1998). *Chem. Commun.* 1067.
[3] Yarks, J., He, L., & Adams, J. D. (2004). *Jr, Pharmacol. Biochem. Behav.*, *78*, 179–183.
[4] Mycek, M. M., Harvey, R. A., & Champe, P. C. (1997). *Pharmacology,* 2nd ed., Lippincott-Raven: Philadelphia.
[5] Zachariadis, P., Hadjikakou, S., Hadjiliadis, N., Michaelides, A., Skoulika, S., Ming, Y., & Xiaolin, Y. (2003). *Inorg. Chim. Acta.*, *343*, 361–365.
[6] Chohan, Z., Rauf, A., Noreen, S., Scozzafava, A., & Supuran, C. (2002). *J. Enzyme Inhib. Med. Chem.*, *17*, 101–106.
[7] Osinsky, S., Levitin, I., Campanella, L., & Wadman, P. (2004). *Exp. Oncol.*, *26*, 140–144.
[8] Chernyavskaya, A. A., Loginova, N. V., Polozov, G. I., Shadyro, O. I., Sheryakov, A. A., & Bondarenko, E. V. (2006). *Pharm. Chem. J.*, *40*, 413.
[9] Singh, K., Barwa, M. S., & Tyagi, P. (2006). *Eur. J. Med. Chem.*, *41*, 147.
[10] Phaniband, M. A., & Dhumwad, S. D. (2007). *Transit. Met. Chem.*, *32*, 1117.
[11] YU, L. C., Lai, L., Xia, R., & Liu, S. L. (2009). *J. Coord. Chem.*, *62*, 1313.
[12] Sheldrick, G. M. (1997). *SHELXS-97. Program for the Solution of Crystal Structures*, University of Gottingen.

[13] Sheldrick, G. M. (1997). *SHELXL-97. Program for Crystal Structures Refinement*, University of Gottingen.
[14] Farrugia, L. J. (1999). *J. Appl. Crystallogr.*, *30*, 837.
[15] (2002). *Stoe & Cie, X-AREA (Version 1.18) and X-RED32 (Version 1.04)* Stoe & Cie, Darmstadt.
[16] Spek, A. L. (2009). *Acta Crystallogr.*, *D 65*, 148.
[17] Frisch, M. J. *et al.* (2004). *Gaussian 03W, Revision C.02.* Gaussian Inc: Wallingford.
[18] Schlegel, H. B. (1982). *J. Comput. Chem.*, *3*, 214–218.
[19] Hohenberg, P., & Kohn, W.(1964). *Phys. Rev.*, *136*, B864–B871.
[20] Becker, A. D. (1993). *J. Chem. Phys.*, *98*, 5648–5652.
[21] Lee, C. *et al.* (1988). *Phys. Rev.*, *B 37*, 785–789.
[22] Frisch, A. *et al.* (2000). *Gauss View User Manual*, Gaussian Inc: Pittsburgh, PA.
[23] Glendening, E. D., Reed, A. E., Carpenter, J. E., & Weinhold, F. (1998). *NBO version 3.1*, TCI, University of Wisconsin: Madison.
[24] Hökelek, T., Dal, H., Tercan, B., Tenlik, E., & Necefoğlu, H. (2010). *Acta Cryst.*, *E66*, m891–m892.
[25] Hökelek, H., Dal, H., Tercan, B., Tenlik, E., & Necefoğlu, H. (2010). *Acta Cryst.*, *E66*, m910–911.
[26] Necefoğlu, H., Özbek, F. E., Öztürk, V., Tercan, B., & Hökelek, T. (2011). *Acta Cryst.*, *E67*, m887–m888.
[27] Bernstein, J., Davis, R. E., Shimoni, L., & Chang, N.-L. (1995). *Angew. Chem. Int. Ed. Engl.*, *34*, 1555–1573.
[28] Fleming, I. (1976). *Frontier Orbitals and Organic Chemical Reactions*, Wiley: London
[29] Kim, K. H., Han, Y. K., & Jung, J. (2005). *Theo. Chem. Accounts.*, *113*, 233.
[30] Aihara, J. (1999). *Theo. Chem. Accounts.*, *102*, 134.
[31] Grabowski, S. J., & Leszczynski, J. (2006). Unrevealing the Nature of Hydrogen Bonds: π – electron delocalization shapes H-bond features, chapter in: *Hydrogen Bonding- New Insights* (Slawomir, J., Grabowski, Kluwer, Academic Publishers).
[32] Tomasi, J., Mennucci, B., & Cammi, R. (2005). *Chem. Reviews.*, *105*, 2999.
[33] Scrocco, E., & Tomasi, J. (1978). *Adv. Quantum. Chem.*, *11*, 115–121.
[34] Luque, F. J., Lopez, J. M., & Orozco, M. (2000). *Theor. Chem. Acc.*, *103*, 343–345.
[35] Politzer, P., Laurence, P. R., Jayasuriya, K., & McKinney, J. (1985). *Special issue of Environ Health Perspect.*, *61*, 191–202.
[36] Scrocco, E., Tomasi, J. (1973). *Topics in Current Chemistry*, 7. Springer Verlag:Berlin, 95.
[37] Grabowski, S. J., & Leszczynski, J. (2006). *Unrevealing the Nature of Hydrogen Bonds: π – electron delocalization shapes H-bond features, chapter in: Hydrogen Bonding- New Insights (J. Slawomir, Grabowski, Kluwer*, Academic Publishers)
[38] Snehalatha, M., Kumar, C. R., Hubert, J. I., Sekar, N., Jayakumar, V. S., (2009). *Spectrochim. Acta.*, *A 72*, 654–662.
[39] Szafram, M., Komasa, A., Adamska, E. B.(2007). *J. Mol. Struct.*, *827*, 101–107.
[40] Coe, B. J. *et al.*, (2005). *J. Am. Chem. Soc.*, *127*, 4845.
[41] Kanis, D. R., Ratner, M. A., & Marks, T. J. (1994). *Chem. Rev.*, *94*, 229.
[42] Bella, S. Di. (2001). *Chem. Soc. Rev.*, *30*, 355.
[43] Lacroix, P. G. Eur. (2001). *J. Inorg. Chem.*, 339.
[44] Long, N. J.(1995). *Angew. Chem., Int. Ed. Engl.*, *34*, 21.
[45] Costes J. P., Lamere, J. F., Lepetit, C., Lacroix, P. G., & Dahan, F. (2005). *Inorg. Chem.*, *44*, 1973.
[46] Coe, B. J., Harris, J. A., Brunschwig, B. S., Asselberghs, I., Clays, K., Garin, J., & Orduna, J. (2005). *J. Am. Chem. Soc.*, *127*, 13399.
[47] Karaer, H., & Gümrükçüoğlu, I. E. (1999). *Turk J. Chem. Cryst.*, *23*61.
[48] Sun, Y. X., Hao, Q. L., Wei, W. X., Yu, Z. X., Lu, L. D., Wang, X., Wang, Y. S. (2009). *J. Mol. Struct.(Theochem).*, *904*, 74–82.